Annual Journal of Hydraulic Engineering,
JSCE VOL. 39 (1995)

Mean and turbulent flows in a single-flood plain open channel

By
Mahmoud F. Maghrebi*, Kiyosi Kawanisi† and Shoitiro Yokosi‡

This paper presents a qualitative and quantitative analysis of the flow in a single-flood plain open channel. A combination of the multi-section flow visualization technique and the Mass-Consistent Model (Sherman[5]) are employed. This shows the mean and instantaneous 3-D behavior of flow interaction, momentum, mass and energy exchange between the main channel and flood plain. The results of mean flow are compared with the ones obtained by a propeller. Investigation of instantaneous flow structures have revealed that the high momentum flow in the main channel is interacted with the low momentum flow in the flood plain. Due to this interaction reversing flow comes out. This causes a subsidiary flow interaction with the surrounding flow in the flood plain. Moreover, comparison of different relative roughs of the flood plain and main channel show that a roughened flood plain generates a stronger secondary current in the main channel while turbulent quantities show larger values in the flood plain.

Keywords : *Compound channel, Flow interaction, Flow visualization*

1. Introduction

In water engineering, many rivers and channels can be found in the shape of compound cross-section or can be modified into one. The problems in compound channels arise from the estimation of the discharge capacity. Conventional methods, usually used to estimate flow discharge of simple cross-sectional shape, do not lead to reliable answers for the channels with compound sections. Depend on the method applied for the estimation of the discharge capacity, the answers will be varied. Some methods lead to overestimated answers while others lead to underestimated answers; reportedly with an error of ±30% (Myers & Brennan [2]). That is why over the years many researchers have tried to find a universal method to estimate the discharge capacity.

An important aspect of flow in compound channels, is the interaction of flow in two adjacent subdivisions (main channel and flood plain). Most of the work on the effect of the interaction of low and high speed regions is restricted to the determination of the velocity distribution, water surface elevation, shear stress over the bed and along the interface plane, and finally important parameters governing the sedimentation problems.

Sequential photographs of the flow and other various techniques of flow visualization have already been used to picture the actual state of flow in real time. However, most of these techniques are restricted to qualitative analysis. The advantages of the conventional quantitative analysis are restricted by limited pictured sections and large time intervals between each loop of photography as well as between sections. The multi-section flow visualization technique with short time interval between consecutive photographs is used to overcome these problems.

Comparison between the results of this method and the ones obtained by various other techniques such as an LDA system or numerical calculation generally show good agreement. Once we checked the reliability of this method, we could go over the instantaneous flow characteristics even though no result could be found for comparison.

The objective of this study is to compare the turbulent flow characteristics in a smooth and roughened flood plain of a compound channel and also to obtain a better understanding of the mechanism of flow interaction between the main channel and flood plain.

*Student Member, Dept. of Civil Engineering, Hiroshima University, 1-4-1 Kagamiyama, Higashi Hiroshima 724
†Member, Res. Assoc., Dept. of Civil Engineering, Hiroshima University, 1-4-1 Kagamiyama, Higashi Hiroshima 724
‡Member, Prof., Dept. of Civil Engineering, Hiroshima University, 1-4-1 Kagamiyama, Higashi Hiroshima 724

2. Experimental condition and procedure

The present experiments were carried out in a free surface water channel. The working section dimensions of the channel were 30.0 m, 0.8 m and 0.12 m in length, width and depth, respectively. At the channel inlet, a bell-mouth and multi-hole steel screens were installed to shape the flow. In order to provide the uniformity of flow, the slope of the water surface and channel slope were arranged to be equal. The coordinate system is right-handed with origin located on the bed at the edge of the flood plain. As is the convention in hydraulics, x, y are horizontal directions and z is vertical one; and u, v, and w are velocity components in the x, y, and z directions, respectively. The height of the flood plain is 6 cm and its width is 40 cm which is equal to half of the channel width.

The experiments were conducted in two cases of smooth and roughened flood plains with smooth main channel, called S-1 and R-1, respectively. For the case of R-1, a rough artificial carpeting material with an equivalent sand roughness of $k_s = 2$ mm was used. The total height of the bankful for two cases were kept equal. The total length of bankful was 6.0 m with a parabolic end at the upstream position, which maintained minimal disturbance.

In order to assess the hydraulic condition of the flow, a miniature propeller current meter of 5 mm in diameter was used. Then, the obtained mean streamwise velocity over the compound cross-section was chosen as a reference velocity (i.e. $U_{ref} = U_m$). In the main channel and flood plain, at each transverse position measurements were performed at 6 and 4 elevations, respectively. The measurements were done in two different transverse sections in the testing area with a longitudinal distance of 40 cm. The obtained data were interpolated over the cross-section using best fit cubic-spline function and then the flow rate was computed as the integral velocity component over the cross-sectional area. The discharge rate of each subdivision was calculated by integrating the velocity distributions.

In flow visualization technique, Nylon beads with diameter of about 0.5 mm and specific density of 1.01 were used as tracers. Such tracers were small enough to outline the smallest organized structures able to be detected in terms of image processing accuracy and space resolution applied to obtain the interpolation data over the grid points. They were first mixed in a water tank installed over the channel and supplied to the water flow at a position 4 m upstream of the testing area.

A projector light was passed through a slit to produce a light sheet at the test sections, 5 mm in depth and approximately 450 mm in the streamwise direction. The light sheet was aimed at a mirror synchronized with a step motor (see Fig. 1). Still photographs were taken by the aid of four cameras, using Fuji photo films with a sensitivity of 1600 ASA. The experimental technique is explained in Kawanisi et al.[3]. The results obtained in this way were used in analysing the flow behavior at $z/H = 0.17 \sim 1.83$.

In the next step, variational technique, developed by Sherman[5], is used to solve numerical equivalent of the flow in the integral approach. In most physical problems it would be formed based on energy consideration. The specific functional which is needed to minimize the variance of the difference between the adjusted values and the original values in non-divergent condition is

$$F(U,V,W,\lambda) = \int_{\forall} \left[{\alpha_1}^2 (U-U_0)^2 + {\alpha_2}^2 (V-V_0)^2 + {\alpha_3}^2 (W-W_0)^2 + \lambda \left(\frac{\partial U}{\partial x} + \frac{\partial V}{\partial y} + \frac{\partial W}{\partial z} \right) \right] d\forall, \tag{1}$$

where U, V, W are the adjusted instantaneous velocity components; U_0, V_0 are the original data obtained directly from image processing; $\alpha_1, \alpha_2, \alpha_3$ are weighting parameters; λ is the Lagrange multiplier, and $\forall$ is the volume of interest. The associated Euler-Lagrange equations whose solution minimizes Eq. (1) are

$$U = U_0 + \frac{1}{2{\alpha_1}^2} \frac{\partial \lambda}{\partial x}, \tag{2}$$

$$V = V_0 + \frac{1}{2{\alpha_2}^2} \frac{\partial \lambda}{\partial y}, \tag{3}$$

$$W = W_0 + \frac{1}{2{\alpha_3}^2} \frac{\partial \lambda}{\partial z}, \tag{4}$$

$$\frac{\partial U}{\partial x} + \frac{\partial V}{\partial y} + \frac{\partial W}{\partial z} = 0. \tag{5}$$

These equations are subject to the boundary conditions

$$\lambda = 0 \quad \text{or} \quad \partial\lambda/\partial n = 0, \tag{6}$$

where n is the outward positive unit normal of the boundary surface. Substituting Eqs. (2)-(4) into (5), the equation for λ is obtained in a Poisson form:

$$\frac{\partial^2 \lambda}{\partial x^2} + \left(\frac{\alpha_1}{\alpha_2} \right)^2 \frac{\partial^2 \lambda}{\partial y^2} + \left(\frac{\alpha_1}{\alpha_3} \right)^2 \frac{\partial^2 \lambda}{\partial z^2} = -2{\alpha_1}^2 \left(\frac{\partial U_0}{\partial x} + \frac{\partial V_0}{\partial y} + \frac{\partial W_0}{\partial z} \right). \tag{7}$$

Since the original vertical velocity component w_0 is unknown we assumed that $w_0 = 0$. This equation was solved by the use of SOR, so a 3-D velocity field over the domain of interest, a broken rectangular box confined on two sides by the channel bed at bottom and water surface at top, could be obtained, which hereafter is called 'frame'.

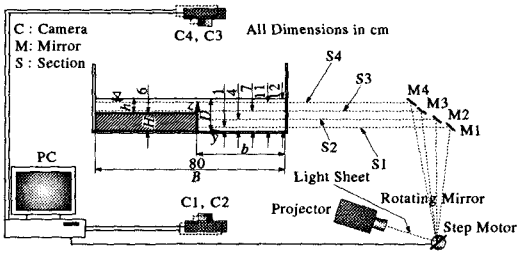

Fig. 1 Schematic sketch of channel cross-section and experimental setup (a downstream end view).

Table 1: Hydraulic conditions and important parameters

Test	Flood Plain	Slope	Discharge				Mean Velocity			
(1)	(2)	(3)	q (l/s) (4)	q_1/q (5)	q_2/q (6)	q_3/q (7)	U_m(cm/s) (8)	U_{1m}/U_m (9)	U_{2m}/U_m (10)	U_{3m}/U_m (11)
S-1	smooth	0.001	10.91	0.324	0.364	0.312	15.2	0.972	1.086	0.934
R-1	rough	0.001	10.67	0.344	0.369	0.287	14.8	1.033	1.108	0.863

3. Mean flow

3-1 Propeller results

Important hydraulic parameters and the results of computed discharge obtained by the use of the propeller are given in Table. 1. The special geometry of channel ($h/H = 1, b/B = 0.5$) guides us to divide the compound channel into three subdivisions with the same area which are named s1, s2 and s3. A schematic sketch of this is shown in Table. 1. This table shows that in the case of S-1, about 1/3 of flow is carried by s1 and interaction effects between s1 and s2 are very small. The dissimilarity of flow regimes between s1 and s2 is very small and only this effect at the majority of the junction border and main channel wall becomes considerable, as will be shown later. In the case of R-1, the percentage of flow carried by s3 is reduced. Almost no considerable change has occurred in s2, so the additional flow is carried by s1. It seems that the interaction effects between s2 and s3 are transferred to s1.

Experimental data prepared by the propeller were used in calculation of depth-averaged velocity profile $\overline{U}/U_m$ and turbulent intensity u'/U_m. On each figure the abscissa is the distance from the intersection of junction border and main channel bed, normalized by the bankful height H.

In Figs. 2 (a, b) the results of depth-averaged velocity profile and turbulent intensity u' for the cases of S-1 and R-1 are given. In the case of S-1, mean flow in the flood plain which is close to the wall at $y/H = -4.4$ and also which is close to the junction edge at $y/H = -0.4$, reaches to its maximum, i.e., $\overline{U}/U_m \simeq 0.9$. In this case no big velocity discontinuity over the junction border can be observed. This data and the ones reported in Keller & Rodi[4] suggest that as h/H increases, discontinuity over the junction decreases. Almost the same pattern can be observed for the case of R-1 with slightly smoother peak. The effect of increasing the relative roughness of the flood plain and main channel can be observed in the reduction of the mean velocity over the flood plain; it shows a decrement of $0.2U_m$ when compared to S-1. The existence of side edge vortices in the flood plain, as mentioned by Tominaga & Nezu[6], causes the reduction of mean velocity at $y/H < -5.0$, whereas the existence of a vortex on the junction edge causes the reduction of mean velocity at $-0.4 < y/H < 1.0$. This phenomenon will be explained later.

The maximum velocity gradient in the vertical direction between s1 and s2 happens in $4.0 < y/H < 5.0$. This can be observed both in S-1 and R-1. The mean velocity in the main channel can be calculated by applying weighting factors of 0.57 and 0.43 to s1 and s2, respectively.

Because of the higher velocity gradient between subsections s1 and s2 from the case S-1, and s2 and s3 from the case R-1, we are expected to have a higher degree of interaction between these subdivisions. In Figs. 2 (c, d) the results of depth-averaged turbulent intensities u' corresponded with the ones of Figs. 2 (a, b), are given. In the case of S-1 (Fig. 2 (c)) the magnitude of turbulent intensity in the flood plain almost distributed uniformly except close to the junction edge; where disturbance due to the interaction of flow between the flood plain and main channel exists.

By comparing cases S-1 and R-1, it can be seen that in the case of S-1, the turbulent intensity in the flood plain is not as large as the case of R-1, although the mean velocity is larger. In the case of R-1, the maximum turbulent intensity occurs at the mid-span of the flood plain (i.e. $y/H = -3.3$). Now consider this quantity in the main channel. Some similarities between the patterns of u' in the lower part of the main channel (s1) can be observed, however, it shows larger values for the case of S-1 as a result of higher velocity. For the upper part of the main channel (s2), the turbulent intensities in the mid-span of main channel are very close to each other. However a sudden increase can be observed when approaching the side walls especially near the junction border. The higher degree of dissimilarity of flow regimes between two adjacent subdivisions of s2 and s3 causes a higher discontinuity in turbulent intensity.

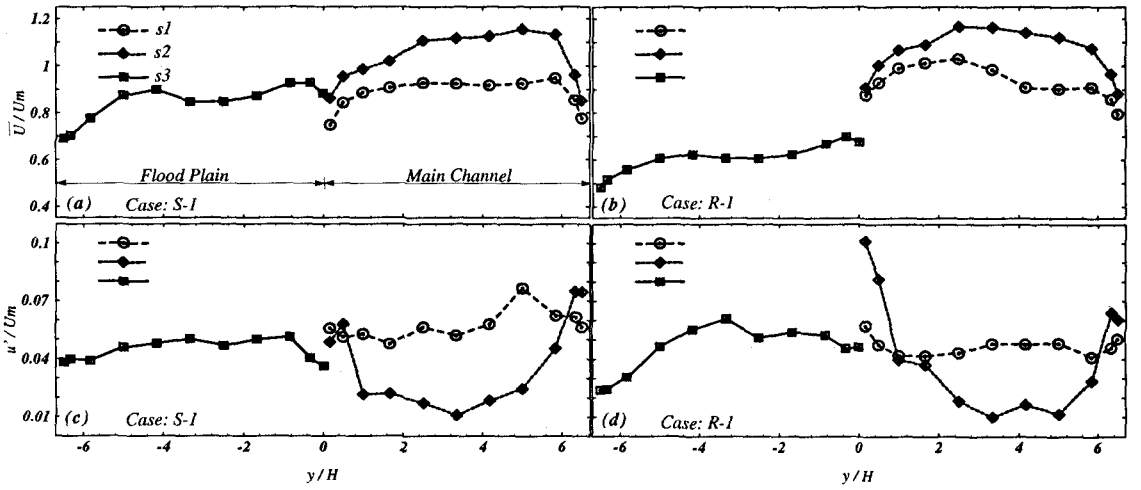

Fig.2 Depth-averaged streamwise velocity and turbulent intensity u' in the compound channel for two cases of S-1 and case R-1

3-2 Flow visualization results

It has always been difficult to investigate secondary flows, because the magnitudes of velocity components contributing to secondary flows are much smaller than the streamwise velocity component.

For each case, we have obtained 15 consecutive frames of instantaneous velocity fields. Two approaches are employed to calculate the mean characteristics of flow. It should be noted that the flow visualization photographs do not cover the whole cross section. First, a mean frame can be obtained by summing up the corresponding values of a grid point in different frames and dividing the result by the number of frames, this can be called the time-averaged method. This method is used to investigate the instantaneous fluctuation quantities along the streamwise direction. Second, all of the experiments have been performed in a uniform flow condition. Therefore, there is practically no discrepancy in different cross-sections, and it is reasonable to use time- and space-averaged values when looking at flow from a cross-section view. For this purpose the following equation has been used:

$$\overline{\overline{f(\mathbf{V})}} = \frac{1}{L}\int_0^L dx \frac{1}{T}\int_0^T f(\mathbf{V})dt, \tag{8}$$

where f is an arbitrary function, $\mathbf{V}$ velocity vector field, L is the total length of integration along the main flow direction, T is the total time interval and symbol $^=$ refers to the time and space averaged values.

The total length of data processing in the main flow direction is 37 cm, mean velocity over the compound cross-section is $U_m = 15.2$ cm/s (in the case of S-1) and the total period of photography for 15 consequent frames is $(15-1)\times 0.5 = 7.0$ s. So one can easily imagine that using equation (8) would be almost equal to the use of a number of three-component current meters, exactly 357 probes (number of grid points in the cross-section), if they were used on grid points in the cross-section instantaneously. The total time of measurement would be $37 \times 7.0/15.2 \simeq 17.0$ s, with a sampling frequency of $37 \times 15/17.0 \simeq 32$ Hz.

Figs. 3 (a, b) show iso-velocity lines of the mean velocity in the main flow direction in the background and vector field of v and w components of velocity mapped on the contour lines in front for the cases of S-1 and R-1, respectively. Although the actual time of measuring is short, the obtained results are reliable and compatible with other work in this field. It seems that two factors lead to favorable results: (1)the method of integration (time-space-averaged method) and (2) variational technique which modifies the incorrect data. In this study, the results of Figs. 3–6 are obtained by the use of time-space average method.

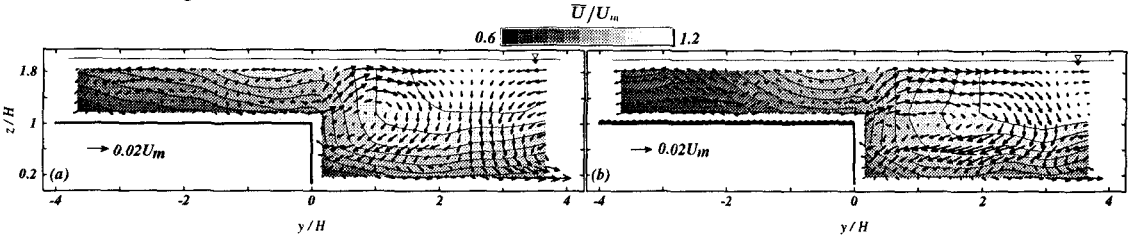

Fig. 3 Time-space-averaged values of u component of velocity (contour lines) and v and w components of velocity (vectors): (a) case S-1 and (b) case R-1

Two main secondary flows can be observed in the main channel of Fig. 3 (a). The one near the junction border has a clockwise sense of rotation and the other, which is likely restricted to the side wall of the main channel ($y/H = 6.7$), has the counter-clockwise direction of rotation. The spanwise size of the secondary flow next to the junction border is $2.5H$. The size of the other secondary flow must be larger than this one. Another secondary flow which is smaller in size can be observed close to the main channel bed next to the junction border. It seems that this secondary current is affected by the larger secondary flow. Therefore, the rotation direction of this smaller one is opposite than that of the larger one.

At the junction point toward the water surface upward flow can be seen, with an angle of 45° to the horizontal direction. An imaginary surface, which passes through the junction point and inclined upward flow, is considered as the interface plane. Fig. 3 indicates that the main part of upward flow is inclined toward the main channel.

In the flood plain two secondary currents can be observed, one being beside the main channel with a counter-clockwise sense of rotation which is almost restricted to $-1.5 < y/H < 0.2$. Next to this at $y/H < -1.5$ another smaller secondary current flow can be observed with the same sense of rotation. Almost identical secondary flow patterns were observed by others namely Tominaga & Nezu[6]) using numerical and experimental approaches. The maximum velocity components of secondary flow is 0.01–$0.03U_m$ which is comparable with the one obtained by Tominaga & Nezu (they have used U_{max} for normalization), though the hydraulic conditions are not exactly the same.

By comparing Fig. 3 (a) with Fig. 3 (b) the effect of adding roughness on the flood plain can be identified. From Fig. 3 (b) it is obvious that the secondary flow in the main channel is extended as far as $y/H = 3.0$ and the area of maximum streamwise velocity is increased. It can also be observed that the streamwise velocity contours are inclined to the main channel. This is possibly caused by a low speed flow as transferring from the flood plain to the main channel. In the flood plain, although the centers of rotating areas are not so clear, stronger secondary current at $y/H < -1.8$ can be observed. This is accompanied with a lower streamwise velocity. In the flood plain the magnitude of vortices contributing in the secondary flow is increased (Maghrebi et al.[1]). Next to this, it seems that the secondary flow is divided into two currents, each with the same sense of rotation in the flood plain. Only one secondary flow, next to the junction border, can be observed.

Fig. 4 shows the iso-lines of advection terms due to secondary currents (it is preferably called "the lateral transfer of momentum by the secondary currents", because the channel is wide enough), calculating $\overline{V}\frac{\partial \overline{U}}{\partial y} + \overline{W}\frac{\partial \overline{U}}{\partial z}$ on grid points normalized by U_m^2/H. As seen, in Fig. 4 (a) the highest lateral transfer of momentum is taken place near the junction point along the interface plane. Low and high momentum flows over the junction border, mainly along the interface plane, exchange momentum with each other and each one takes on the characteristics of a momentum balanced flow. Along the interface plane they go up toward the water surface. Going up along the interface plane, the width of the mixing region increases. In the upper regions, low and high momentum flows have two alternatives. They can either rotate over the flood plane or turn back into the main channel. Almost identical patterns can be observed for the roughened flood plain however, with a higher momentum gradient.

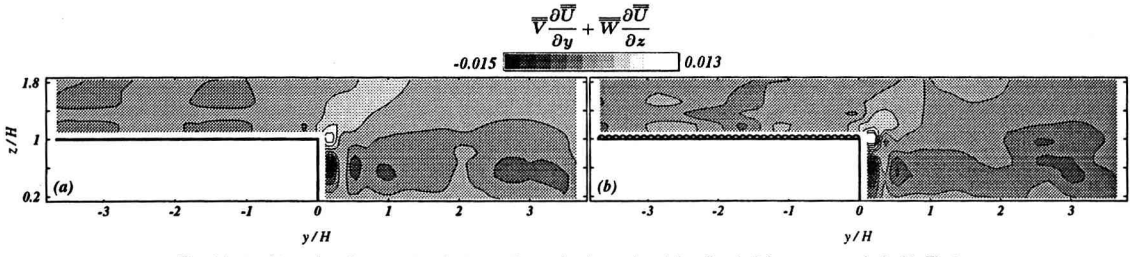

Fig. 4 Lateral transfer of momentum between the main channel and the flood plain corresponded with Fig.3

4. Turbulent flow

4-1 Turbulent intensities

Fig. 5 shows the turbulent intensities u', v' and w' for cases of S-1 and R-1 normalized by the corresponded U_m, respectively. By considering Figs. 5 (a, b), at a glance, similar patterns can be found in two cases specially close to the walls in the main channel and flood plain. Close to the walls the highest turbulent intensities can be observed. They are stretched along the walls. Comparing the two cases of S-1 and R-1, one can see that in the case of R-1, due to the stronger secondary currents, the turbulent intensity u' is driven to higher extend in the main channel. In the case of S-1 the value of u' is larger than the case of R-1. There is a good compatibility between the turbulent intensity u' and v'.

The patterns of v' in comparison to w' seem very simple. From Figs. 5 (c, d) it is obvious that the iso-lines of v' are located over each other and seem to be stratified. This shows a linear decrement from the bed to the water surface. The minimum value of v' does not occur attached to the water surface but below it at $z/H = 0.17 \simeq 1.5$. An important fact

regarding this comparison is that the turbulent intensity v' for the case of R-1 is larger than S-1.

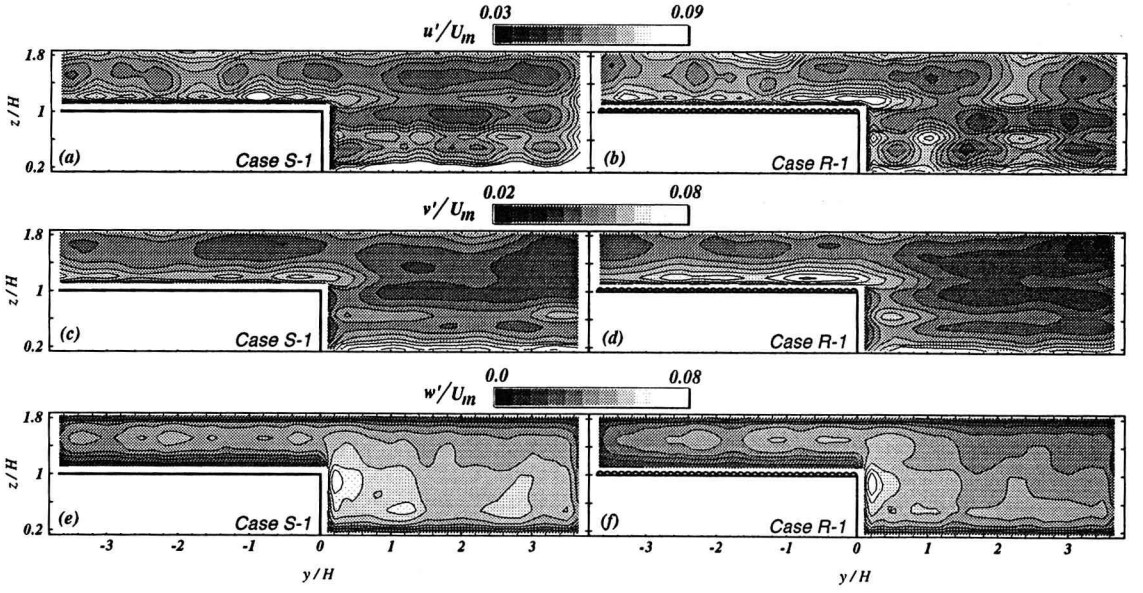

Fig.5 Time-space-averaged turbulent intensities U', $V'$and W' for two cases of S-1 and case R-1

The results of Figs. 5 (c, d) and (e, f) can be compared with each other in three ways: first, between v' and w', second, between the cases of S-1 and R-1 and third, between the flood plain and main channel. The keyword for interpretation is the degree of freedom of flow in the y- and z-directions. Over the flood plain, the degree of freedom for velocity components in the y-direction is much larger than in the z-direction, because the flow in the z-direction is restricted to the bed and water surface, whereas in a comparative wide channel like the one at hand, the confined effects of side wall can be ignored. Apart from this the applied boundary condition for the top and bottom of the flow were in such a way that $W = 0$ so the values of v' is larger in comparison to w'.

Beds in the main channel for both cases of S-1 and R-1 are smooth and local velocities in S-1 are larger than R-1, whereas the flood plains have different roughs. This shows a particular effect specially on the flood plain and along the interface plane. Adding roughness to the flood plain disturbs the flow and this increases the fluctuation velocity components and consequently the turbulent intensities.

The minimum value of w' can be observed close to the walls and water surface. The presence of wall prevents large fluctuations in the z-direction. Next to the junction border in the main channel the maximum value of w' happens. As going to the main channel the intensity of w' decreases. It is of particular importance to note that on the flood plain, the contour-lines are stretched along the flood plain while next to the junction border it is along the junction border. In the main channel the depth of flow is as large as twice the one in the flood plain. Therefore, it is expected to have larger values of w' in the main channel in comparison with the ones in the flood plain. Frankly speaking, because of the applied boundary condition the results related to the w compounded of velocity can not be reliable when located close to the bed and water surface. From Figs. 5 (e, f), close to the junction border high values of w' can be observed. Recalling Fig. 4, the contribution of w component of velocity in momentum exchange is evident, it mainly happens in the main channel close to the junction border.

4-2 Turbulent energy and Reynolds stresses

Figs. 6 (a, b) show the iso-lines of the turbulent kinetic energy $k = (u'^2 + v'^2 + w'^2)/2$ which is normalized by the corresponded U_m^2. The same patterns as seen in u' can be observed here. This implies the fact that the dominant component of kinetic energy is u'. Here, unlike the primary mean velocity in Fig. 3 whose the isovels bulge along the upward flow, an extension from the flood plain to the main channel can be observed.

Figs. 6 (c, d) and (e, f) show the turbulent Reynolds stresses $-\overline{uv}$ and $-\overline{uw}$ for the two cases of S-1 and R-1 normalized by the corresponded U_m^2, respectively. From Figs. 6 (c, d), in the flood plain and close to the junction edge, the contour-lines are stretched along the y-axis. The maximum value of $-\overline{uv}$ can be observed along the interface plane at the junction edge in the main channel and the high Reynolds stress can be observed at $y/H = 0.8$. It seems that when two secondary currents approach each other on the intersection border where induced velocity is created, Reynolds stress $-\overline{uv}$ shows a

higher value.

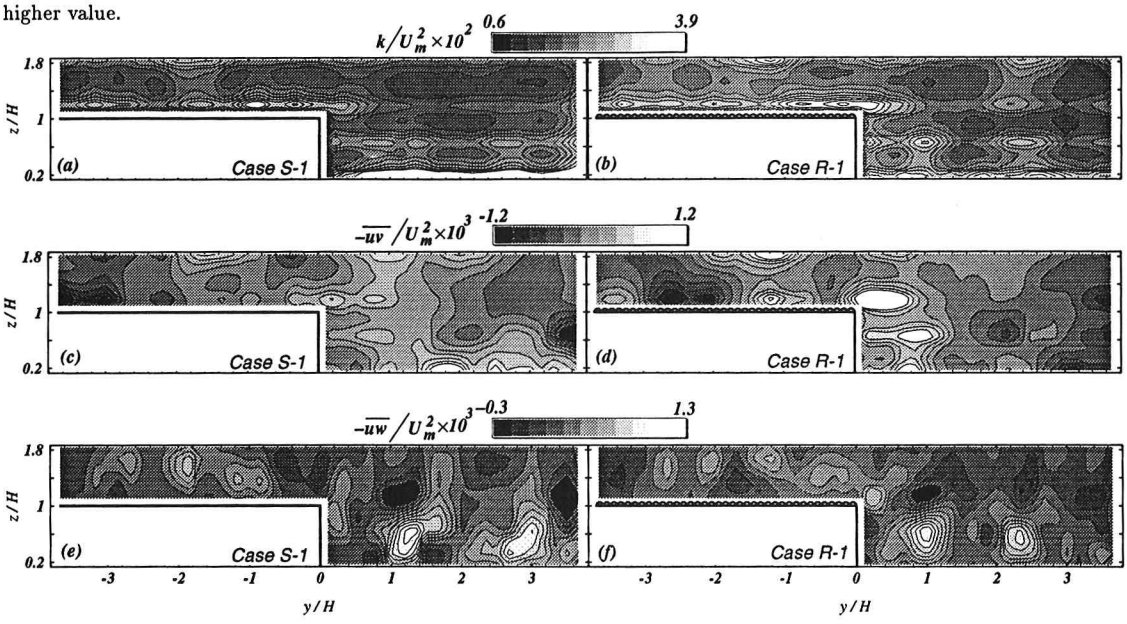

Fig.6 Time-space-averaged turbulent energy k=($u'^2+v'^2+w'^2$) /2 and Reynolds stresses $-\overline{uv}$ and $-\overline{uw}$

Figs. 6 (e, f) show the iso-lines of the turbulent Reynolds stress $-\overline{uw}$ which are normalized by the corresponded U_m^2. The iso-lines are stretched in the z-direction. The magnitude of stretching in the case of S-1 is larger than R-1. As mentioned before, the disturbance in the flood plain mostly appears in v component of velocity, therefore larger values of $-\overline{uv}$ to be found in the main channel. Although general compatibility can be observed in turbulent quantities (shown in Figs. 5 and 6 and those reported by Tominaga & Nezu [6]), their results are larger than ours. It should be noted that the measurements of these authors include the whole spectrum of the turbulent motions while the present work resolves only the larger-scale fluctuations.

5. Instantaneous flow characteristics

5-1 Velocity fluctuations

Discussion of the instantaneous behavior of flow helps us to further explore the mechanism of flow transfer, interaction and hidden characteristics of flow which are impossible to be identified just by investigating the mean flow. Because of the stronger secondary currents which were found in the case of R-1 (frame number 12), special attention should be given regarding the result of this case. Here we have given two longitudinal sections close to the junction border, and one horizontal section which passes through the main channel and flood plain.

Having obtained the 3-D frames of all components of the instantaneous velocities, it is now possible to calculate a time-averaged frame. The average velocity in x-direction is calculated based on the following equation:

$$\overline{U}_{i,j,k} = \frac{1}{n}\sum_{t=1}^{n} U^t_{i,j,k}, \tag{9}$$

where t is the frame number, n is the total number of frames , i, j and k refer to the grid numbers in x, y and z-directions, respectively and $\overline{U}_{i,j,k}$ is time-averaged velocity in the main flow direction at (i, j, k). Similarly, using the above equation two other components of mean velocity $\overline{V}_{i,j,k}$ and $\overline{W}_{i,j,k}$ can be obtained. The mean frame obtained in this way is used in calculation of the velocity fluctuations. Fig. 7 (a) shows a longitudinal view of an instantaneous fluctuation vector field exactly over the junction edge (i.e. at $y/H = 0$). Many of the vectors, especially those close to the junction edge, are stretched towards downstream, whereas at the upper parts close to the water surface the reverse flow can be observed. It should be mentioned once more that the interface plane is not located in the vertical direction but makes an angle of 45° to the $+y$-direction passing through the junction edge. Consequently, the flow in the lower parts which is closer to the interface plane, is affected largely by the high momentum flow in the main channel.

Another longitudinal section of instantaneous fluctuation velocity components of u and w is given in Fig. 7 (b). The vector pattern at the upper parts close to the water surface is the same as what we have for Fig. 7 (a). However, from the bankful elevation to the lower parts of the main channel, a rotating flow with a clockwise sense of rotation can be seen at $x/H \approx 2.0$. Fig. 7 (c) shows a horizontal section of instantaneous fluctuations of u and v components of velocity

at $z/H = 1.33$. It is clear that along the interface plane (at this elevation it can be considered at $y/H = 0.33$), the high momentum flow from the main channel is interacted with low momentum flow in the flood plain. Due to this it loses its speed. Therefore they can be seen as returning to the flood plain at $x/H = 3.0$. The interaction of low and high momentum flows leads to the rotating flow which implies the direct effect of continuity in flow. The center of this rotating flow can be marked at $x/H = 2.6$ and $y/H = -0.7$. As this low momentum flow interacts with a higher momentum flow in the flood plain, a subsidiary rotating flow farther from the junction border is created; so a couple of rotating flows can be observed in $-1.7 < y/H < 0.3$. The size of the rotating area is limited to $2H$ in the spanwise-direction and $4H$ in the longitudinal-direction. A schematic sketch of this phenomenon is shown in Fig. 7 (d).

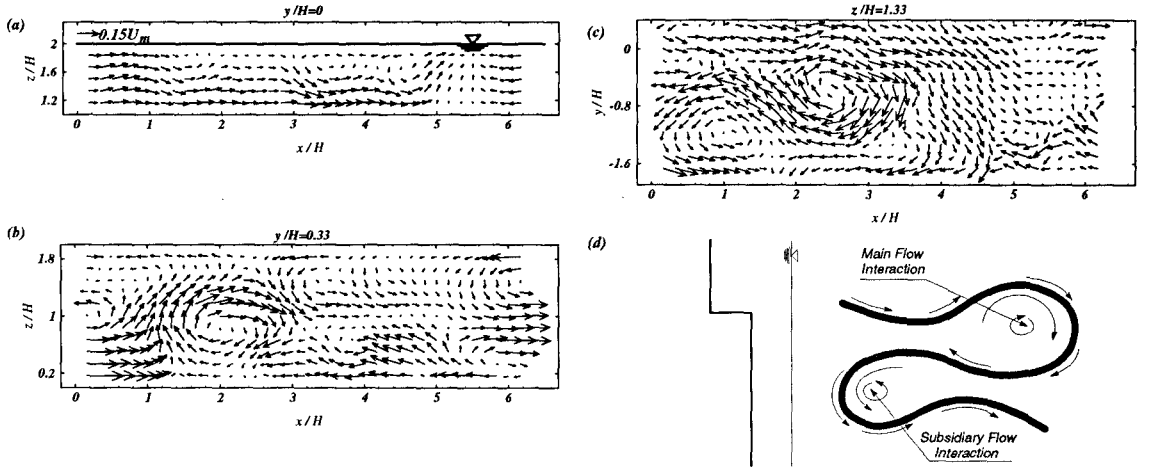

Fig. 7 Velocity fluctuations in two longitudinal sections (a,b) and a horizontal section (c) of the case R-1 and (d) schematic sketch of flow interaction

6. Summary and final conclusions

In order to investigate the 3-D phenomenon of flow interaction in a compound channel and also to discover the mechanism of momentum exchange between the flood plain and main channel, the instantaneous 3-D velocity fields were continuously obtained by the use of the multi-section flow visualization technique and Mass-Consistent Model.

With the multi-section flow visualization, in order to obtain the maximum amount of information, the number of pictured sections is increased to four. Then, a very rapid sequential photographs were taken using a step motor. Using this technique, problems related to synchronization were overcome.

Comparison of two cases of smooth and roughened flood plain shows that in the case of roughened flood plain the secondary flow driven from the flood plain to the main channel extends to a higher lateral depth in the main channel. The other point is that the v and w components of velocity contributed in the secondary flow are larger. The turbulent intensities and Reynolds stress $-\overline{uv}$ over the roughened flood plain are larger than the smooth case, whereas Reynolds stress $-\overline{uw}$ is larger in the main channel close to the junction border.

Investigation of instantaneous flow structures have revealed that the high momentum flow in the main channel is interacted with the low momentum flow in the flood plain. Due to this interaction reversing flow comes out. The reduced momentum flow once more participates in an interaction with the surrounding flow in the flood plain. This leads to a subsidiary flow interaction. Through this process which continuously happens in compound channel, mass and momentum are exchanged between the main channel and the flood plain.

REFERENCES

1) Maghrebi, M. F., Kawanisi, K. and Yokosi S. 1994 On the behavior of vortical structures in a single-flood plain open channel, *Journal of the Visualization Society of Japan,* **14**, No.55.

2) Myers, W. R. C. and Brennan, E. K. 1990 Flow resistance in compound channels. *Journal of the Hydraulics Research,* **28**, 141–155.

3) Kawanisi, K., Maghrebi, M. F. and Yokosi, S. 1993 An instantaneous 3-D analysis of turbulent flow in the wake of a hemisphere. *Boundary Layer Meteorology,* **64**, No.1/2.

4) Keller, R. J and Rodi, W. 1988 Prediction of flow characteristics in main channel/flood plain flows. *Journal of Hydraulic Research.* **26**, 425–441.

5) Sherman, C. A. 1978 A mass-consistent model for wind fields over complex terrain. *Journal of Applied Meteorology* **17**, 241–253.

6) Tominaga, A. and Nezu, I. 1991 Turbulent structure in compound open-channel flows. *Journal of Hydraulics Engineering, ASCE* **117**, 21–41.